

Remote sensing of ephemeral water bodies in western Niger

J. P. VERDIN

U.S. Geological Survey, EROS Data Center, Sioux Falls, South Dakota 57198, U.S.A.

(Received 17 November 1994; in final form 29 May 1995)

Abstract. Research was undertaken to evaluate the feasibility of monitoring the small ephemeral water bodies of the Sahel with the 1.1 km resolution data of the National Oceanic and Atmospheric Administration (NOAA) Advanced Very High Resolution Radiometer (AVHRR). Twenty-one lakes of western Niger with good ground observation records were selected for examination. Thematic Mapper images from 1988 were first analysed to determine surface areas and temperature differences between water and adjacent land. Six AVHRR scenes from the 1988-89 dry season were then studied. It was found that a lake can be monitored until its surface area drops below 10 ha, in most cases. Furthermore, with prior knowledge of the location and shape of a water body, its surface area can be estimated from AVHRR band 5 data to within about 10 ha. These results are explained by the sharp temperature contrast between water and land, on the order of 13°C.

Résumé. On a étudié la possibilité de suivre les mares temporaires du Sahel à l'aide des données au 1.1 km de résolution du Radiomètre Avancé à Haute Résolution (AVHRR) des satellites de la série NOAA. Vingt et un mares du Niger Occidental titulaires de bonnes données de terrain furent choisis pour cette étude. Les données du Thematic Mapper (TM) de 1988 furent d'abord analysées afin de déterminer les superficies des dits lacs et les différences de température entre l'eau et la terre. Six scènes AVHRR prises pendant la saison sèche de 1988-89 ont ensuite été étudiées. Il s'est avéré que dans la plupart des cas il est possible de suivre un lac tant que sa superficie reste supérieure à 10 ha. De plus, quand l'emplacement et la forme du lac sont déjà connus, la superficie du lac peut être estimée à partir des données de la bande 5 du AVHRR à environ 10 ha près. La forte différence de température, d'environ 13°C, entre l'eau et la terre rend possible ce suivi et ces estimations.

1. Introduction

The Agriculture-Hydrology-Meteorology (AGRHYMET) programme of West Africa is carried out by the nine member countries of the Comité Inter-Etats de Lutte contre la Sécheresse au Sahel (CILSS): Burkina Faso, Cape Verde, Chad, Gambia, Guinea-Bissau, Mali, Mauritania, Niger, and Senegal. Started in 1975, it contributes to improved food security in the region through the application of agrometeorological and hydrological information. One important function of the programme is the collection and dissemination of data and information regarding the spatial and temporal variability of water and vegetation resources in the Sahel. The marked seasonal and cyclical nature of the meteorological phenomena governing the relative abundance of these resources, and the associated implications for food security in the region, have prompted investment in remote sensing and telecommunications technology. One notable activity in this area is the direct reception of image

data from the National Oceanic and Atmospheric Administration (NOAA) polar-orbiting satellites and the operational production of vegetation index (greenness) maps from them at the AGRHYMET Regional Center (ARC) in Niamey. These greenness maps, produced every 10 days during the rainfed agricultural season, can be interpreted to obtain information describing current conditions of crops and rangeland. This information is disseminated to the National AGRHYMET Centres and other interested parties in the form of maps and bulletins in both analog and digital form.

While the greenness maps provide insight into the condition of grazing lands, additional information regarding the availability of surface water would increase the AGRHYMET programme's ability to guide the movements of pastoralists and their flocks. There are many small, ephemeral water bodies scattered throughout the region that are used for watering livestock. Their relative fullness, or even presence, is quite variable and difficult to predict due to the vagaries of rainfall distribution and the characteristically high evaporation rates in the Sahel. High-resolution remote sensing systems, such as Landsat Thematic Mapper (TM) and the *Système Pour l'Observation de la Terre* (SPOT), permit unambiguous identification of these water bodies, but the associated data volumes, expense, and lack of timeliness make them impractical sources for operational monitoring. For these reasons, there has been a long standing interest at the ARC in the development of a hydrological index from readily available NOAA Advanced Very High Resolution Radiometer (AVHRR) imagery, similar to the normalized difference vegetation index (NDVI), which is the basis for greenness mapping. The present study was undertaken as a first step in evaluating the feasibility of monitoring these water bodies with the 1.1 km resolution imagery from the AVHRR instruments on the NOAA polar orbiters.

2. Previous work

Images from Earth-observing satellites have been used to survey surface water resources since the early days of the Landsat programme. Work and Gilmer (1976) showed that the spectral bands of the 80-meter resolution Landsat Multi-Spectral Scanner (MSS) were suitable for detection of prairie lakes and ponds in the Dakotas down to 1.6 ha. Best and Moore (1979), also working in the Dakotas, showed that reliable regional statistical models could be developed to estimate small water body volumes from areas determined with Landsat MSS images. Eckhardt and Litke (1988) surveyed water bodies in Colorado with Landsat MSS and SPOT High Resolution Visible (HRV) (20 m resolution) images, detecting ponds as small as 0.5 ha and 0.1 ha, respectively.

In the Sahel, the recent cooperative work carried out under the auspices of the Comité Interafricain d'Études Hydrauliques (CIEH), and reported by Piaton and Puech (1992), is especially relevant to the present study. They reported that SPOT HRV images can be used to inventory water bodies as small as 0.25 ha, with a localization to within 50 m, if topographic maps at scales of 1:50 000 or 1:100 000 are available to provide geometrical control. They showed that evaporation is the primary factor of the hydrological budget governing the shrinkage of surface water bodies during the October–May dry season. From these findings, they demonstrated that depth-area and depth-volume equations can be fit for a water body, given three observations of area during a dry season. Thereafter, for any year of interest, surface areas and volumes for any date during the dry season can be calculated, given basic evaporation data and a determination of the water body's surface area at the outset

of the dry season. The importance of these findings to the present study will become evident in later sections of this paper.

Studies employing imagery from the 1.1 km resolution AVHRR to survey surface water extent are far fewer than for the imagery provided by the Landsat and SPOT satellites. Notable are the results of Harris and Mason (1989), who used AVHRR observations to estimate the surface area (390 km²) of Lough Neagh, a lake in Northern Ireland. They obtained a precision of 1 per cent of true area using daytime band 2 (near-infrared) and night-time bands 4 and 5 (thermal infrared) data, which for their study site offered the best contrast between water and land.

3. Study area

A number of considerations contributed to the selection of a study area for the investigation. An area with a relatively high density of ephemeral lakes was sought, within a reasonable distance from Niamey to permit the option of field visits. The availability of cloud-free Landsat and AVHRR imagery was also a basic criterion, with preference given to the 1988 time frame, because this was the wettest year in recent history in the region. Under such conditions, the lakes would be at their greatest surface area, maximizing their detectability with the AVHRR. The final selection of the study area was determined by the results presented by Piaton and Puech (1992), which included the locations, surface areas (ranging from 1 to more than 150 ha), topographic profiles, and the calibration of area-elevation equations for some 30 water bodies in the region around Tillabery. Figure 1 shows the study area as defined by the extent of the Landsat TM quarter scene that encloses it. The Niger river transects the study area from north-west to south-east, and there are three major areas of irrigated agriculture along its eastern bank. To the east of the

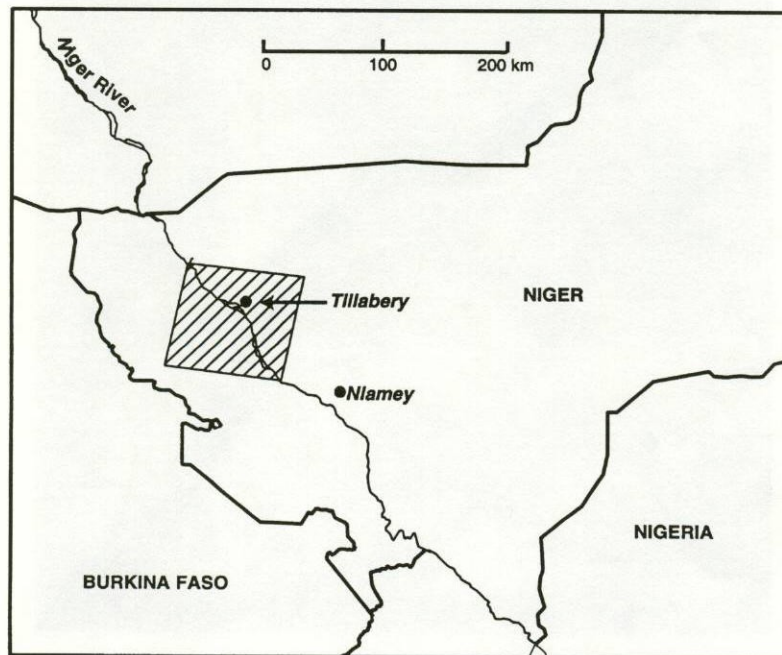


Figure 1. Location of the study area in western Niger.

river, the terrain is dominated by dissected lateritic uplands, with the ephemeral water bodies found in the drainage networks that have been incised there. On the west side of the river, there are some areas of laterite, but the region is characterized more by permanent dunal structures which are extensively used for rainfed agriculture. Many ephemeral water bodies occur in the interdunal depressions. In general, vegetative cover is sparse, with its relative vigour varying according to the abundance of seasonal rains. The northward shift of the Intertropical Convergence Zone brings rain during the months of May through September, and from October through to April there is virtually no rain at all.

4. Selection of Landsat TM images

The first priority in selecting TM images was to find coverage of the calibrated lakes of the CIEH study at peak of fullness at the end of the 1988 rainy season. This requirement was met by the TM scene at Path 193, Row 50, of the Worldwide Reference System 2 (WRS2), which was acquired by Landsat-5 on 8 October 1988, and recorded at the ground receiving station at Fucino, Italy. Only the south-west quadrant of the scene was used. The image is cloud free and reveals the presence of scores of minor water bodies in the area. It was geometrically corrected at the U.S. Geological Survey's Earth Resources Observation Systems (EROS) Data Center to fit the Lambert Conformal Conic projection. Figure 2 presents band 5 (middle infrared) of the scene in geocorrected format. Water bodies appear as distinct dark objects against a light background of soil, rock, and vegetation.

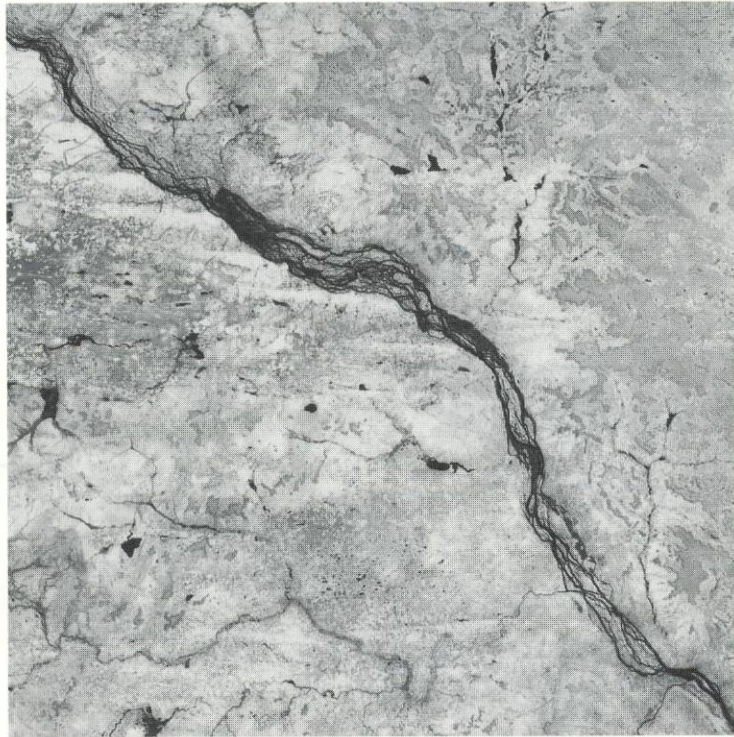


Figure 2. Landsat TM band 5 of 8 October 1988, at WRS 193/50, south-west quadrant, resampled to Lambert Conformal Conic projection.

A second Landsat TM image was obtained to document the condition of water bodies at the end of the dry season, when their surface areas would be at a minimum. This would demonstrate, along with the 8 October 1988 image, the two extremes of surface water presence. Ideally, a scene would have been obtained from early May 1989, at the end of the dry season which followed the acquisition of the 8 October 1988, TM scene. The beginning and ending conditions of the period of AVHRR image analysis would have been well documented. Unfortunately, no such image was available. A quarter scene acquired by Landsat-4 on 9 May 1988, was obtained instead from EOSAT in Lanham, Maryland, U.S.A. It is cloud free and was resampled to the same projection grid as the October scene. It documents the low water conditions preceding the 1988 rainy season (see figure 3).

5. Analysis of TM imagery

The analysis of TM imagery addressed two objectives: the determination of 1988 surface areas of lakes for which area-elevation equations were calibrated in the CIEH study, and the determination of differences in apparent surface temperature between the lakes and the surrounding land. Both efforts served to support the analysis of AVHRR scenes from the October 1988 to May 1989 time period.

Surface area determination was performed using band 5 (1.55–1.75 μm , middle infrared), which offers the best contrast between water and land of any of the TM bands (figure 4). The method for calculating the area of a lake from histogram information was the same as that presented by Piaton and Puech (1992) and Harris

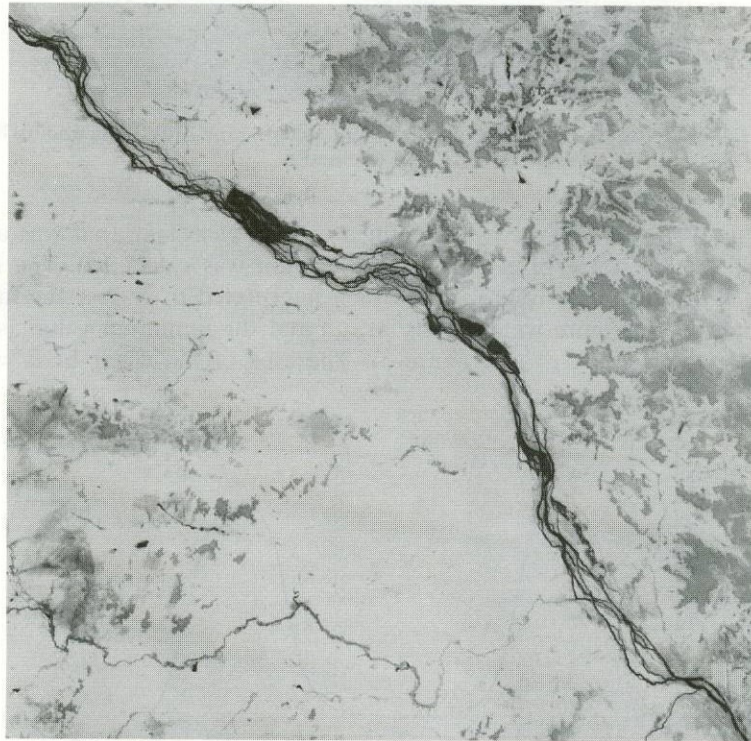


Figure 3. Landsat TM band 5 of 9 May 1988, at WRS 193/50, south-west quadrant, resampled to Lambert Conformal Conic projection.

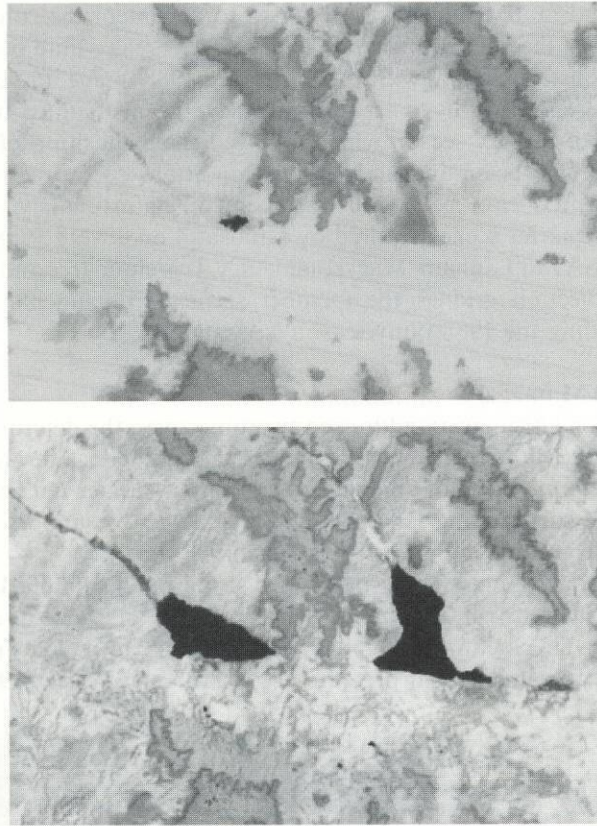


Figure 4. Lakes 23 (right) and 24 (left) as they appeared on (a) 9 May 1988, and (b) 8 October 1988, in TM band 5.

and Mason (1989). A window was identified around each lake that was about 50 per cent filled with water pixels, and the histogram was calculated. The resulting histogram, being distinctly bimodal, was then interpreted to choose the maximum value associated with pure water pixels (W_{max}) and the minimum value associated with pure land pixels (L_{min}) (see figure 5). The area of the water body was then

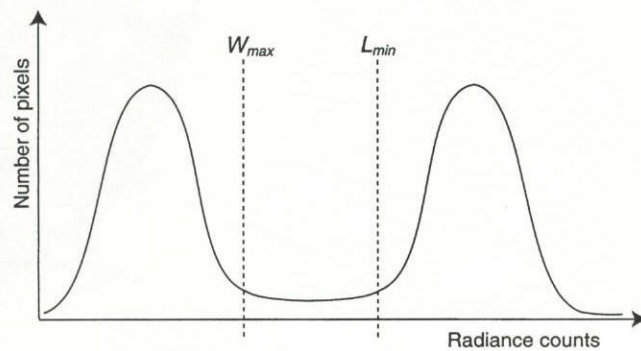


Figure 5. Typical histogram for a TM band 5 window centred on a water body.

obtained by multiplying the area of a pixel (30 m by 30 m, or 0.09 ha) times the number of pure water pixels, plus half the number of pixels lying between W_{\max} and L_{\min} . This was done for 21 lakes of the CIEH study that could be confidently located in the TM scenes. Results were obtained for both the 9 May and 8 October scenes of 1988 (table 1), and show that significant increases in surface area occurred between these dates (see figure 4).

TM band 6 lies in the thermal infrared (10.4–12.5 μm) and has a spatial resolution of 120 m. It corresponds spectrally to bands 4 and 5 of the AVHRR (10.3–11.3 and 11.5–12.5 μm , respectively), which have 1.1-km resolution. TM band 6 was examined to gain insight into the kinds of information that might be obtained by processing AVHRR bands 4 and 5. Specifically, the data were examined interactively at a computer screen to read off values within and adjacent to lakes in the study area, to quantify the temperature contrast between water and land. Digital counts were converted to apparent temperatures using the calibration equation presented by Markham and Barker (1986). The difference in apparent surface temperature between water and land was found to be about 13°C for those cases where water surface area is great enough to give a signal without land radiance contamination (about 15 ha by inspection).

6. Selection and preprocessing of AVHRR imagery

The goal in selecting AVHRR scenes was to obtain a set of cloud-free images spanning the period 1 October 1988, to 31 May 1989, to process and analyse to determine the nature of the detectable signal from water bodies of known location. Selection also took into account the satellite-look angle, with every effort made to

Table 1. Surface areas of water bodies determined from TM band 5 of 9 May and 8 October, 1988.

USGS No	CIEH name	9 May 88 area (ha)	8 October 88 area (ha)
3	TIL 3	0.0	7.7
5	GOT 9	11.3	69.8
6	GOT 4	0.0	13.8
7	GOT 8	0.6	14.7
8	GOT 5	0.0	12.4
12	DAR 6	0.0	11.6
21	TIL 4	4.2	54.2
22	TIL 6	34.7	93.1
23	TIL 6 bis	2.3	178.6
24	TIL 6 ter	7.8	150.3
25	TIL 11	12.6	53.5
26	TIL 15B	2.9	12.9
27	TIL 15A	9.9	22.1
28	TIL 16	0.0	8.1
29	TIL 16bis	0.0	13.2
30	TIL 17	44.0	161.9
32	TIL 22	25.7	45.4
34	TIL 1aC	0.0	95.7
35	TIL 1bB	15.7	147.9
36	TIL 1cA	0.0	13.8
37	DAR 4	36.9	40.4

Table 2. Selected AVHRR images for water body signal analysis. Angles refer to averages over the study area.

Image date	NOAA satellite	Satellite zenith angle (°)	Solar zenith angle (°)
4 October 1988	9	15	62
21 October 1988	9	11	69
13 November 1988	11	42	38
11 December 1988	11	5	44
31 December 1988	11	4	42
8 May 1989	11	12	25

choose scenes having the study area near the nadir position of the instrument scan. Table 2 summarizes the six daytime scenes that were selected. The gap between the 31 December 1988, and 8 May 1989, acquisition dates is explained by the fact that this period is outside the time of the AGRHYMET Program's agricultural monitoring campaign, and, therefore, no scenes were recorded at the station in Niamey. The scenes for 4 October 1988, and 8 May 1989, contain some cloud cover but were retained to have useful imagery for the beginning and end of the dry season.

Geometrical correction was done in a way to facilitate comparison with the TM images. First, the TM scene of 8 October 1988, was coarsened to approximate AVHRR spatial resolution. This was done by passing an 18 pixel by 18 pixel window over the 30 meter TM band 5 geocorrected data (see figure 2) and calculating the local average. The resulting image (figure 6) has a 540 m resolution. This image was then used in image-to-image registration procedures with the clearest and most geometrically sound AVHRR scene, that of 31 December 1988 (figures 7 and 8). Land-water interfaces were used as control. The remaining AVHRR scenes were geocorrected by image-to-image techniques using the corrected 31 December 1988, as the standard. Radiometric correction was applied as described by Teillet and Holben (1994). Each image consists of 195 lines of 223 pixels, each pixel representing a 540 m square.

7. Analysis of AVHRR imagery

Land and water discrimination is most commonly done using data from the near infrared portion of the spectrum (0.7–1.3 μm , for example, SPOT band 3, TM band 4, Landsat MSS bands 3 and 4, and AVHRR band 2). Water is highly absorbent in these wavelengths, and soil, rock, and vegetation are generally quite reflective, giving good contrast between the target of interest and its background. AVHRR band 2 was, therefore, the first band examined in this study. Dark areas were found to correspond to water bodies, as expected, but the lateritic upland areas were found to exhibit a very similar signature. (Compare figure 7 with figure 2). This confusion led to consideration of other AVHRR bands for water body monitoring. Piaton and Puech (1992) reported similar problems in the Tillabery region with SPOT band 3 and were able to overcome them by employing instead the NDVI computed from SPOT bands 2 and 3. They reported that NDVI images offered a superior differentiation between laterites and water with high concentrations of suspended sediments. This was not found to be the case, however, for the NDVI calculated from AVHRR bands 1 and 2. It was found to offer no significant advantage over the AVHRR

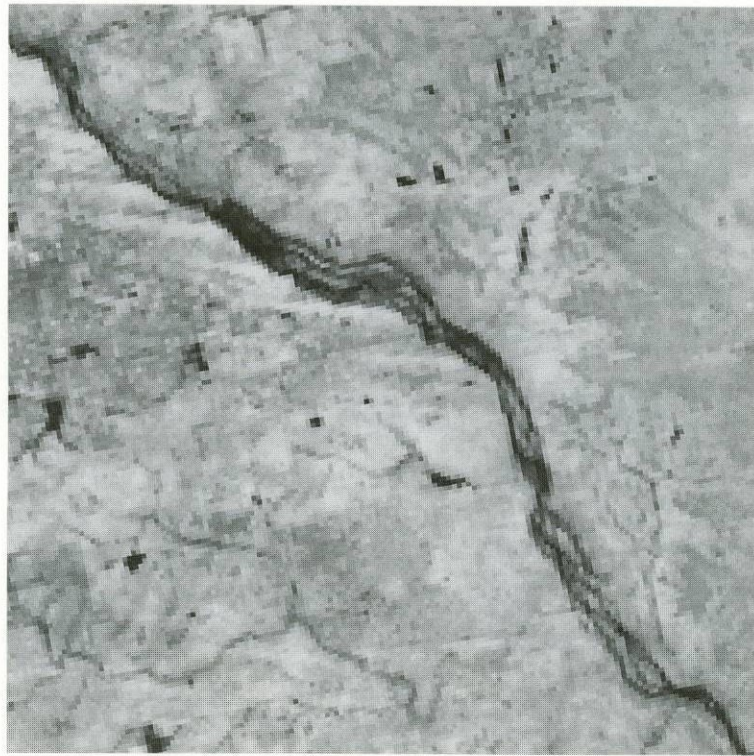


Figure 6. Landsat TM band 5 of 8 October 1988, averaged over 18-by-18 windows to yield 540 m pixels.

band 2, perhaps because of complications due to coarse spatial resolution. AVHRR band 1 also was found to have similar responses for laterites and surface water.

As stated earlier, the TM band 5 offers the best discrimination between water and land of the bands on that sensor. There is no direct analog to TM band 5 on the AVHRR, but a subtraction of AVHRR band 4 from AVHRR band 3 has been shown to yield a synthetic band 6 with similar properties. It has been useful in other parts of the world (Holroyd *et al.* 1989). Band 3 responses contain a mix of emitted (thermal infrared) and reflected (middle infrared) energy, and the subtraction of the band 4 response, which is due entirely to emitted energy, leaves the reflected component of band 3. Although this reasoning ignores differences in emissivity between bands 3 and 4, the technique has proven practical for scenes with highly contrasting targets. A synthetic band 6 was calculated for the scenes of this study. Although it did offer a good definition of cloud pixels, and better land and water discrimination than AVHRR bands 1, 2, and NDVI due to reduced confusion with laterites, it still could not match the discrimination offered by AVHRR thermal bands 4 and 5 (compare figure 8 with figures 7 and 2).

Visually, no practical difference was noted between bands 4 and 5 for the images studied, and so band 5 was adopted as the band that would be employed. For the 21 lakes identified in the TM scenes, calibrated by the CIEH, for which surface area estimates had been made from the TM image of 8 October 1988, a systematic examination of the AVHRR band 5 signals was undertaken at their known locations.



Figure 7. AVHRR band 2 (reflective infrared) of 31 December 1988, resampled to Lambert Conformal Conic projection.



Figure 8. AVHRR band 5 (thermal infrared) of 31 December 1988, resampled to Lambert Conformal Conic projection.

For each lake and for each of the six dates of AVHRR scenes, a subjective classification of the signal at each point was made. Surface water is relatively cool and so appears much darker than land. The signal was called strong if a distinct, dark cool spot was evident, and weak if water was present but with a reduced contrast relative to the surrounding land. A determination of no signal was made if there was no discernible difference in response between the point and the ambient land surface. Many lakes were seen to influence the signal of groups of several pixels (each representing about 29 ha, especially at the outset of the dry season, in spite of their surface area being less than the 120 ha resolution of the AVHRR sensor. For each successive image date in the dry season, fewer and fewer lakes had detectable signals. This was expected, because evaporation causes the surface areas of the lakes to shrink steadily with time. Table 3 presents the results of this visual classification.

The depth-area relations presented by Piaton and Puech (1992) for the 21 lakes of table 3 is

$$S = S_0 H^\alpha \quad (1)$$

where S is the surface area (in hectares) on a day with depth H (in metres), S_0 is the surface area (in hectares) when the depth is 1 m, and α is an exponent fit for a series of observations of S and H . Values of α are typically around 1.25 for the small water bodies of the Sahel.

For the 21 lakes with known surface areas for 8 October 1988, (see table 1) and values of S_0 and α , the depth H on that day can be calculated with equation (1). From that date forward during the dry season, evaporation data can be used to calculate reductions in H , and, in turn, (1) can be used to calculate the corresponding surface area, S . During October and November, H must be reduced by infiltration in addition to evaporation. Piaton and Puech (1992) suggest a rate of 2 mm per day, except for lakes ringed by live trees or having contact with a high infiltration rate overflow zone early in the dry season. They recommend a rate of 3 mm per day for these latter conditions, which in the present study apply only to water bodies 21 (TIL 4) and 23 (TIL 16 bis). Mean daily evaporation rates, by month, for 1978–89 at Tillabery (Piaton and Puech 1992) were employed, along with the infiltration rates, to reduce the initial (8 October 1988) H values for each lake forward in time to the dates corresponding to AVHRR image acquisition. The surface area estimates yielded by equation (1) for these dates are presented in table 4.

Joint examination of tables 3 and 4 permits identification of the surface area interval in which water bodies become no longer detectable by AVHRR band 5. The comment column of table 3 summarizes these observations, which can be generalized as indicating that most water bodies disappear once they drop below a size on the order of 10 ha in area. It is difficult to be more exact in this regard, given the sources of uncertainty due to the use of historical mean daily evaporation rates (rather than actual rates), approximate infiltration rates, and fitted equations relating area and depth. The practical significance of these findings is the clear indication that subpixel sized water bodies can be resolved by the AVHRR due to the sharp contrast between the surface temperature of the water bodies and that of the surrounding land.

Dozier (1981) showed that for a pixel representing an area composed of two distinct temperature fields, the radiance in an AVHRR thermal band depends on the portion of the pixel area occupied by each field, that is:

$$L(T) = pL(T_t) + (1 - p)L(T_b) \quad (2)$$

Table 3. Visual classification of strength of water body signals in AVHRR band 5.

No	Name	4 October 1988 signal	21 October 1988 signal	13 November 1988 signal	11 December 1988 signal	31 December 1988 signal	8 May 1989 signal	Comment
3	Til 3	N	N	N	N	N	N	8, never visible
5	Got 9	W	W	W	W	W	W	still visible at 25
6	Got 4	W	W	W	W	W	W	12→9 disappears
7	Got 8	W	W	W	W	W	W	still visible at 0
8	Got 5	W	W	W	W	W	W	10→7 disappears
12	Dar 6	cloud	W	W	W	W	W	8→6 disappears
21	Til 4	W	W	W	W	W	W	33→11, disappears
22	Til 6	W	W	W	W	W	W	still visible at 50
23	Til 6 bis	S	S	S	S	S	S	still visible at 76
24	Til 6 ter	S	S	S	S	S	S	still visible at 70
25	Til 11	W	W	W	W	W	W	33→8 disappears
26	Til 15B	N	N	N	N	N	N	13, never visible
27	Til 15A	N	N	N	N	N	N	22, never visible
28	Til 16	cloud	W	W	W	W	W	8, never visible
29	Til 16 bis	N	N	N	N	N	N	13, never visible
30	Til 17	W	W	W	W	W	W	still visible at 81
32	Til 22	W	W	W	W	W	W	32→14 disappears
34	Til 1aC	W	W	W	W	W	W	36→0, disappears
35	Til 1bB	W	W	W	W	W	W	111→58, disappears
36	Til 1cA	W	N	N	N	N	N	14→11, disappears
37	Dar 4	W	W	W	W	W	W	17→13, disappears

S = strong signal W = Weak signal N = No signal

Table 4. Surface areas (ha) of water bodies on AVHRR acquisition dates after 8 October 1988, estimated by (1).

No	Name	8 October 1988 area	21 October 1988 area	13 November 1988 area	11 December 1988 area	31 December 1988 area	8 May 1989 area
3	Til 3	7.7	6.4	4.5	2.9	2.0	0.0
5	Got 9	69.8	65.9	59.6	53.5	50.2	25.4
6	Got 4	13.8	11.7	8.7	6.1	4.8	0.0
7	Got 8	14.7	7.8	0.0	0.0	0.0	0.0
8	Got 5	12.4	10.2	7.2	4.7	3.5	0.0
12	Dar 6	11.6	10.2	8.0	6.0	4.9	0.0
21	Til 4	54.2	50.3	42.8	36.4	33.3	11.2
22	Til 6	93.1	89.8	84.5	79.2	76.2	50.4
23	Til 6 bis	178.6	170.2	156.7	143.3	135.9	76.2
24	Til 6 ter	150.3	143.8	133.3	122.9	117.1	70.3
25	Til 11	53.5	49.5	43.1	36.8	33.4	7.5
26	Til 15B	12.9	11.5	9.4	7.3	6.3	0.0
27	Til 15A	22.1	20.4	17.6	15.0	13.5	2.6
28	Til 16	8.1	6.7	4.6	2.6	1.6	0.0
29	Til 16 bis	13.2	11.4	8.2	5.4	4.1	0.0
30	Til 17	161.9	155.3	144.8	134.3	128.6	81.1
32	Til 22	45.4	42.9	38.7	34.6	32.3	14.3
34	Til 1aC	95.7	83.1	63.6	45.5	36.2	0.0
35	Til 1bB	140.8	140.8	129.2	117.6	111.3	58.2
36	Til 1cA	13.8	11.5	8.2	5.5	4.2	0.0
37	Dar 4	40.4	34.3	25.1	17.1	13.1	0.0

where L is upwelling thermal radiance ($\text{W m}^{-2} \mu\text{m}^{-1} \text{sr}^{-1}$), T is temperature (K), t indicates the target temperature field, b indicates the background temperature field, and p is the proportion of the pixel area occupied by the target temperature field. Calibrated AVHRR thermal band data represent radiant temperatures according to the transform:

$$T = \frac{\text{DN}}{2} + 202.5 \quad (3)$$

where T again is the temperature (K) and DN refers to the digital numbers as read from a corrected image file. In the narrow range of temperatures of interest, 298 to 313 deg K, L and T are essentially linearly related, so (2) can be rewritten as:

$$\text{DN} = p\text{DN}_t + (1 - p)\text{DN}_b \quad (4)$$

In the case of the Sahel, the background temperature field is that of the land surface, and the target temperature field is that of surface water. An estimate of p for a pixel of interest, can be obtained with a knowledge of DN_b and DN_t . DN_b is readily determined by examining the land pixels surrounding a water body. DN_t can be determined from a water body in the scene having a great enough extent to exhibit a pure water response. In the present study, the widest reach of the Niger river was used.

If the portion of a pixel occupied by surface water can be estimated by equation (4), then it is only one more step to exploit this to estimate the surface area of a water body. The pixel area, 540 m by 540 m or 29 ha is multiplied by the proportion of water, and such values are summed for all pixels corresponding to the water body. This procedure was applied to 13 lakes appearing in the AVHRR scene of 4 October 1988. Table 5 presents the results of this exercise, along with areas derived from the TM scene of 8 October 1988, for comparison. It is seen that for water bodies greater than 15 ha the AVHRR band 5 estimates are within 25 per cent of the correct value. The mean error in absolute terms, over all 13 lakes, is 11 ha. Although the sample is small, the errors do not show a consistent over- or under-estimation. Relative errors, naturally, are greater for the smaller water bodies.

Table 5. Surface areas (ha) of 13 lakes estimated from AVHRR band 5 of 4 October 1988, with TM band 5 areas of 8 October 1988.

USGS No	CIEH Name	NOAA 4 October 1988	TM 8 October 1988	PCT diff	HA diff
5	Got 9	60	70	-14	-10
6	Got 4	33	14	136	19
7	Got 8	21	15	40	6
8	Got 5	10	12	-17	-2
21	Til 4	50	54	-8	-4
22	Til 6	73	93	-22	-20
23	Til 6 bis	169	179	-6	-10
24	Til 6 ter	156	150	4	6
25	Til 11	67	54	24	13
32	Til 22	50	45	11	5
34	Til 1aC	90	96	-6	-6
35	Til 1bB	183	148	24	35
36	Til 1cA	8	14	-43	-6

It is important to qualify the favourable results obtained with AVHRR band 5. Prior knowledge of the location and approximate size and shape of a lake is necessary to know which pixels should be included in an area estimation calculation. This can be provided by Landsat or SPOT imagery from dates when lakes are reasonably full. The establishment of appropriate values of DN_b and DN_t requires careful judgement and must be repeated for each scene or subscene of interest, as environmental conditions vary spatially and temporally. The signal for pure water, DN_t , is clearly more difficult to obtain in the Sahel than DN_b . Dozier (1981) showed that by writing equation (2) for both bands 3 and 4, and simultaneously solving them, values for both p and T_t can be determined. The technique requires the use of numerical methods to solve the two simultaneous nonlinear equations. Further research might determine the practicality of an operational implementation of the technique by the AGRHYMET programme.

The application of atmospheric correction techniques, if successful, would make possible the reliable comparison of reflectances and temperatures derived from image data acquired on different dates. Split window techniques used operationally for estimating sea surface temperature overcome atmospheric effects in the thermal bands, but cannot be applied to land surfaces because unknown variations of emissivity must be accounted for. Localized split window solutions have been shown to be possible (Becker and Li 1990, Otlé and Vidal-Madjar 1992), but remain unwieldy for operational implementation.

8. Conclusions

The ephemeral water bodies of western Niger have been shown to have a detectable signal in the AVHRR band 5 data. A lake can be monitored until its surface area drops below 10 ha, in most cases. This is possible due to the temperature contrast between water and land, which is on the order of 13 °C, in spite of the 120 ha resolution of the AVHRR sensor. Furthermore, with prior knowledge of the location, shape and size of a water body, its surface area can be estimated from the AVHRR band 5 data to within approximately 10 ha.

AVHRR bands 1 and 2, and the NDVI calculated from them, were not found to be especially valuable for monitoring the water bodies of the study area. This is due to the confusion between surface water and laterites, the absorbing properties of the latter approaching those of water in these wavelengths.

The ARC has the necessary technical resources to monitor the lakes of this study with AVHRR band 5 imagery. A pilot study in which data are interpreted in near real-time would reveal whether the demonstrated techniques can, indeed, be implemented operationally.

Acknowledgments

Dr Rui Silva defined this study from the point of view of the AGRHYMET programme. At the EROS Data Center, Dr Donald Moore provided valuable technical discussion and advice. Work was performed under USAID Participating Agency Service Agreement No. AFR-0973-P-IC-9014, Sahel Water Data Network and Management III.

References

- BECKER, F., and LI, Z., 1990, Towards a local split window method over land surfaces. *International Journal of Remote Sensing*, **11**, 369–393.

- BEST, R. G., and MOORE, D. G., 1979, Landsat interpretation of prairie lakes and wetlands of eastern South Dakota. *Satellite Hydrology, Proceedings of the Fifth William T. Pecora Memorial Symposium on Remote Sensing, Sioux Falls, South Dakota, U.S.A., August 1979* (Bethesda, MD: American Water Resources Association), pp. 499–506.
- DOZIER, J., 1981, A method for satellite identification of surface temperature fields of subpixel resolution. *Remote Sensing of Environment*, **11**, 221–229.
- ECKHARDT, D. W., and LITKE, D. W., 1988, Estimation of reservoir surface areas using satellite imagery, Upper Gunnison Basin, Colorado. *Conference on Water Data for Water Resources Management, Tucson, Arizona, U.S.A., August 1988* (Bethesda, MD: American Water Resources Association), pp. 691–702.
- HARRIS, A. R., and MASON, I. M., 1989, Lake measurement using AVHRR, a case study. *International Journal of Remote Sensing*, **10**, 885–895.
- HOLROYD, E. W., VERDIN, J. P., and CARROLL, T. R., 1989, Mapping snow cover with satellite imagery: comparison of results from three sensor systems. *Proceedings of the 57th Western Snow Conference, Fort Collins, Colorado, 18–20 April 1989, Western Snow Conference, Portland, Oregon, U.S.A.* (Portland, OR: The Western Snow Conference), pp. 59–68.
- MARKHAM, B. L., and BARKER, J. L., 1986, Landsat MSS and TM post-calibration dynamic ranges, exoatmospheric reflectances and at-satellite temperatures, Landsat Technical Notes, August, EOSAT, Lanham, Maryland, U.S.A., pp. 3–8.
- OTTLÉ, C., and VIDAL-MADJAR, D., 1992, Estimation of land surface temperature with NOAA9 data. *Remote Sensing of Environment*, **24**, 27–40.
- PIATON, H., and PUECH, C., 1992, Apport de la télédétection pour l'évaluation des ressources en eau d'irrigation pour la mise en valeur des plans d'eau à caractère permanent ou semi-permanent au Niger, Rapport de Synthèse, Série Hydraulique Agricole, Comité Interafricain d'Études Hydrauliques, Laboratoire Commun de Télédétection CEMAGREF/ENGREF, Montpellier, France.
- TEILLET, P., and HOLBEN, B., 1994, Towards operational radiometric calibration of NOAA AVHRR imagery in the visible and infrared channels. *Canadian Journal of Remote Sensing*, **20**, 1–10.
- WORK, E. A., and GILMER, D. S., 1976, Utilization of satellite data for inventorying prairie ponds and lakes. *Photogrammetric Engineering and Remote Sensing*, **42**, 685–694.